Beyond the thermal model in relativistic heavy-ion collisions

Georg Wolschin*

Institut für Theoretische Physik der Universität Heidelberg, Philosophenweg 16, D-69120 Heidelberg, Germany, EU

(Received 21 April 2016; revised manuscript received 31 May 2016; published 17 August 2016)

Deviations from thermal distribution functions of produced particles in relativistic heavy-ion collisions are discussed as indicators for nonequilibrium processes. The focus is on rapidity distributions of produced charged hadrons as functions of collision energy and centrality, which are used to infer the fraction of particles produced from a central fireball as compared with that from the fragmentation sources that are out of equilibrium with the rest of the system. Overall thermal equilibrium would only be reached for large times $t \to \infty$.

DOI: 10.1103/PhysRevC.94.024911

I. INTRODUCTION

The statistical hadronization or thermal model [1] with a limiting temperature $T_{\rm H}$ has been successfully used to reproduce, over the full energy range where data have been measured, the ratios of particle production yields for various hadron species in e^+e^-, pp, and relativistic heavy-ion collisions (see, e.g., Refs. [2–4]). However, a necessary and sufficient condition for attaining thermal equilibrium in particle collisions is provided by the agreement of measured distribution functions with thermal distributions, rather than particle yields.

An example of a thermal distribution may be found in the cosmic microwave background radiation. It has a blackbody spectrum with a temperature of 2.735 K at redshift zero [5], although there are spatial temperature anisotropies on the level of less than 1 part in 10^4 which give rise to structure formation; these have meanwhile been measured with excellent accuracy by, e.g., the Wilkinson Microwave Anisotropy Probe (WMAP) [6] and Planck [7] collaborations.

In relativistic heavy-ion collisions, the distributions of both transverse momentum $p_{\rm T}$ as well as rapidity y (or pseudorapidity η) of produced charged hadrons clearly deviate from thermal distributions. At energies of the BNL Relativistic Heavy-Ion Collider (RHIC) and the CERN Large Hadron Collider (LHC), the deviations in a $p_{\rm T}$ region of $0.5\ {\rm GeV}/c \lesssim p_{\rm T} \lesssim 7\ {\rm GeV}/c$ and the ensuing transition from exponential to power-law $p_{\rm T}$ distributions are usually attributed to collective expansion and nonequilibrium processes. Above $\sim$7 GeV/c, hard events become visible which require a perturbative QCD (pQCD) treatment. When integrated over $p_{\rm T}$ to obtain particle yields, their contribution is negligible but decisive as an indicator for nonequilibrium events.

Traces of nonequilibrium behavior can be found in (pseudo)rapidity distributions of produced charged hadrons as measured by ALICE in PbPb [8] and by ATLAS, ALICE, and LHCb in pPb collisions [9,10]. The distribution functions have important contributions from the fragmentation regions that are clearly visible in net-proton rapidity distributions at CERN Super Proton Synchrotron (SPS) and RHIC energies [11–13], but also contribute to charged-hadron production. For produced particles, they are found to increase in particle content proportional to $\ln(s_{NN})$ and are not in equilibrium with particles produced in the midrapidity source that arises essentially from low-x gluons.

In the following section several indications for nonthermal system properties found in transverse momentum distributions of produced charged hadrons are reviewed. Since it turns out that $p_{\rm T}$ distributions are, however, inadequate to differentiate fragmentation and central fireball contributions, this serves as a motivation for the investigation of rapidity distributions where the respective role of these individual sources is more obvious. The relevance of the fragmentation contributions is reconsidered in Sec. III, followed by the discussion of pseudorapidity distributions at RHIC and LHC energies with emphasis on the equilibration of the three sources in Sec. IV. The conclusions are drawn in the last section.

II. TRANSVERSE MOMENTUM DISTRIBUTIONS

Starting from a purely thermal model for particle production in relativistic heavy-ion collisions, the transverse momentum distribution of produced charged hadrons may be represented by a relativistic generalization of the Maxwell–Boltzmann distribution that accounts for the fact that the velocity of light, c, is an upper limit. The corresponding distribution function was first derived by Jüttner [14] and is therefore called the Maxwell–Juettner distribution:

$$f(p_{\rm T}) = \frac{1}{4\pi m^2 T K_2(m/T)} \exp\left[-\frac{\gamma(p_{\rm T})m}{T}\right], \qquad (1)$$

with the modified Bessel function of the second kind $K_2(m/T)$, the Lorentz factor

$$\gamma(p_{\rm T}) = \sqrt{1+(p_{\rm T}/m)^2}, \qquad (2)$$

freeze-out temperature T, and hadron mass m. Here I take $T \equiv T_{\rm F} = 120$ MeV (without considering collective expansion, which would lead to a larger effective value), and $m \equiv \langle m \rangle$ as the average value of the masses of pions, kaons, and nucleons with contributions of 83%, 13%, and 4%, respectively, that correspond to particle production yields in 2.76 TeV PbPb [15].

This thermal distribution function is compared in Fig. 1 [16] with the charged-hadron distribution measured by ALICE [17] in 2.76 TeV PbPb for three centralities. Here the absolute

*g.wolschin@thphys.uni-heidelberg.de

 ©2016 American Physical Society

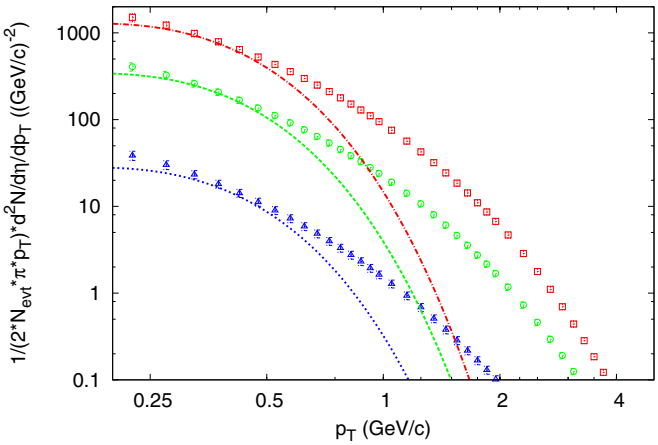

FIG. 1. Jüttner distribution functions of a relativistic thermal Maxwell gas at temperature T without collective expansion compared to measured transverse momentum distributions of produced charged hadrons in 2.76 TeV PbPb collisions from ALICE [17] for 0%–5%, 30%–40%, and 70%–80% centralities (top to bottom; $|\eta| < 0.8$); see text [16].

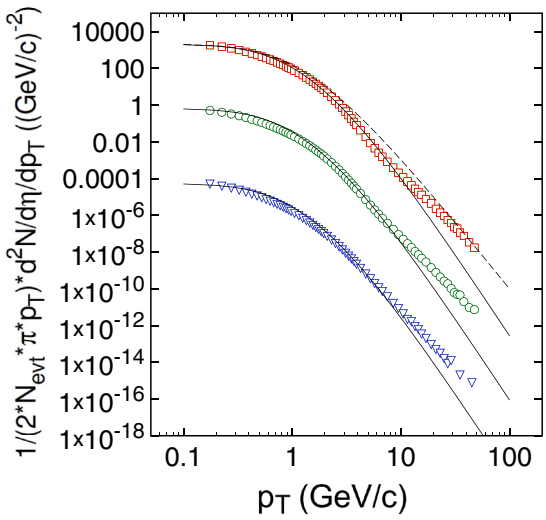

FIG. 2. Transverse momentum distributions of produced charged hadrons in 2.76 TeV PbPb collisions calculated from $f(p_T) \propto [1 + (q-1)m_T/T]^{1/(1-q)}$ compared with ALICE data [17] for 0%–5%, 30%–40%, and 70%–80% centralities (top to bottom). Solid curves are for $q = 1.10$, the dashed curve is for $q = 1.12$. Peripheral spectra are scaled for better visibility; see Fig. 1 for absolute values.

value of the distribution has been adjusted to the measured result at 0%–5%, whereas the normalizations of the calculated distributions at 30%–40% and 70%–80% are obtained from the corresponding ratios of the midrapidity yields [18].

Obviously, the relativistic thermal distributions fit the measured ones only for very small transverse momenta $p_T \lesssim 0.5$ GeV/c. The generally accepted explanation for this failure is that the system expands collectively. The expansion may to some extent be accounted for phenomenologically by a higher effective temperature $T^* = T + m\langle v_T\rangle^2$ [19].

The mean transverse velocity $\langle v_T\rangle$ depends on the transverse temperature profile and the corresponding velocity at freeze-out time, which are both functions of centrality and may be calculated hydrodynamically, yielding an effective temperature of $T^* \simeq 260$ MeV for 0%–5% centrality and a correspondingly broader transverse momentum distribution, which agrees with the experimental values in a mean p_T range.

To treat the transverse expansion in detail, numerous theoretical approaches are available, starting from the blast-wave model [20] and its boost-invariant generalization [21]. More recently advanced hydrodynamical models such as those reviewed in Refs. [22–24] provide a rather complete description of the collective expansion phase.

The p_T distributions clearly show a transition from an exponential behavior in the thermal regime Eq. (1) to a power-law behavior in the p_T range that is attributed mostly to the recombination of soft partons and fragmentation of hard partons. In addition to detailed theoretical approaches, this transition can be modelled phenomenologically by using distribution functions of the form

$$f(p_T) \propto [1 + (q-1)m_T/T]^{1/(1-q)}, \tag{3}$$

with the transverse mass $m_T = (m^2 + p_T^2)^{1/2}$, a freeze-out temperature T, and a dimensionless parameter $q \gtrsim 1$. For $q \to 1$ the exponential distribution (extensive statistics) is recovered, whereas $q > 1$ may be fit to the measured distribution functions.

The functional form (3) can be related to an earlier empirical QCD-inspired result proposed by Hagedorn [25] for high-energy pp and $p\bar{p}$ collisions:

$$E\frac{d^3\sigma}{dp^3} = C(1 + p_T/p_0)^{-n}, \tag{4}$$

with a normalization constant C and parameters p_0, n. Choosing $p_0 = T/(q-1)$, $n = 1/(q-1)$, and replacing p_T by m_T, Eqs. (3) and (4) are found to be equivalent; see also Wilk and Wong [26] for pp. Hence, both expressions describe the transition from exponential [$\propto \exp(-m_T/T)$ for $p_T \to 0$ as in the Jüttner distribution (1)] to power-law behavior [$\propto (p_T/nT)^{-n}$ for $p_T \to \infty$].

Using Eq. (3)—or equivalently, Eq. (4)—Fig. 2 shows calculated p_T distributions of produced charged hadrons for three centralities in 2.76 TeV PbPb compared with ALICE data from Ref. [17] (peripheral spectra are scaled for better visibility; see Fig. 1 for absolute values; statistical and systematic error bars are smaller than the symbol size). Here the freeze-out temperature is $T \equiv T_F = 120$ MeV and the average mass is $m \equiv \langle m\rangle = 0.22$ GeV/c^2, as in Fig. 1.

The data are well represented through many orders of magnitude with $q = 1.10$ (Fig. 2), but above $p_T \sim 7$ GeV/c deviations occur which are attributed to hard processes that require a pQCD treatment. This limiting value of $p_T \sim 7$ GeV/c corresponds to a minimum in the nuclear modification factor for produced charged hadrons as a function of p_T found in Ref. [17].

Better results for the high-momentum tails would be achieved with slightly larger values of q such as $q = 1.12$ corresponding to a power index $n = 8.3$ shown in Fig. 2,

but only at the expense of an unsatisfactory fit at mid-$p_{\rm T}$ values. It thus appears that, apart from hard processes that cannot be treated in a statistical approach, the functions (3) and (4) properly account for the transition from exponential to power-law spectra seen in the measured p_T distributions.

Several authors have argued that distributions with $q > 1$ may reflect nonequilibrium systems with inhomogeneous temperature and long-range interactions; e.g., Ref. [27]. Previously Tsallis [28] had constructed a ("nonextensive") $q \neq 1$ statistics that incorporates Eq. (3) and would only in the absence of correlations assume the Boltzmann form—see, however, Balian and Nauenberg [29] for a critical discussion of this view.

There is presently no convincing theoretical derivation of the value of q—or alternatively, of n—that is needed to reproduce the experimental $p_{\rm T}$ distributions in relativistic heavy-ion collisions. It is therefore not obvious from the present analysis what fraction of low-$p_{\rm T}$ particles is due to nonequilibrium processes that differ from thermal emission out of a single expanding fireball. In particular, one cannot distinguish particles emitted from the fireball and those arising from the fragmentation sources at low $p_{\rm T}$. Hence the analysis of transverse momentum distributions in terms of q spectra is presently only suitable to distinguish high-$p_{\rm T}$ hard events from the bulk of (thermal and nonequilibrium) charged-hadron emission.

III. FRAGMENTATION DISTRIBUTIONS

The distinction of particles emitted from the fireball and those from the fragmentation sources is more transparent in rapidity or pseudorapidity distributions of produced charged hadrons. The existence of the fragmentation sources is evident from the measurements of stopping in heavy-ion collisions: Net-proton (proton minus antiproton) rapidity distributions $dN_{p-\bar{p}}/dy$ exhibit two fragmentation peaks which are strongly overlapping at energies per particle pair of $\sqrt{s_{NN}} \lesssim 20$ GeV, but move apart at higher c.m. energies, leaving a midrapidity valley [30] at RHIC energies of 200 GeV [11] that is predicted to broaden further at LHC energies [12,13]. It is then largely depleted of baryons, with fragmentation peaks occurring in the rapidity regions $y = \mp 5$–7. Stopping is a highly nonequilibrium process which is not suitable for any kind of thermal or equilibrium description.

The fragmentation peaks in stopping occur mainly due to the interaction of valence quarks with soft gluons in the respective other nucleus. Their positions in rapidity space can be obtained from [12]

$$\frac{dN_{p-\bar{p}}}{dy} = \frac{C}{(2\pi)^2}\int \frac{d^2p_{\rm T}}{p_{\rm T}^2} x_1 q_v(x_1,p_{\rm T}) f_g(x_2,p_{\rm T}), \qquad (5)$$

for the peak in the forward region, and a corresponding symmetric contribution for the peak in the backward region that is obtained by replacing $y \to -y$. Here, $x_1 = p_{\rm T}/\sqrt{s}\exp(y)$ and $x_2 = p_{\rm T}/\sqrt{s}\exp(-y)$ are the respective longitudinal momentum fractions carried by the valence quark v in the projectile that undergoes stopping and the soft gluon g in the target. The valence-quark distribution function is $q_v(x_1,p_{\rm T})$ and the gluon distribution $f_g(x_2,p_{\rm T})$ is the Fourier transform of the forward dipole scattering amplitude $N(x_2,r_{\rm T})$ for a quark dipole of transverse size $r_{\rm T}$. The normalization constant C is adjusted such that the integral of Eq. (5) yields the total number of participant protons in net-proton distributions or baryons in net-baryon distributions.

The fragmentation-peak positions $y_{\rm peak}$ in rapidity space are at sufficiently high energy—in particular, at LHC energies—indicators for the gluon saturation scale

$$Q_{\rm s}^2 = A^{1/3} Q_0^2 x^{-\lambda}, \qquad (6)$$

with the mass number A, the momentum scale Q_0, the momentum fraction $x < 1$ carried by the gluon, and the saturation-scale exponent λ.

Rapidity distributions $dN_{p-\bar{p}}/dy$ at SPS and RHIC energies are calculated within the model of Ref. [12] for two values of the gluon saturation scale and compared with net-proton data from SPS and RHIC in Fig. 3 [32]. A larger gluon saturation momentum $Q_{\rm s}$ produces more stopping, as does a larger mass number A. In the context of an investigation of particle production, the agreement between the calculated stopping distributions and the data is taken as evidence for the importance of fragmentation contributions also in charged-hadron production.

The peak positions are found to depend in a large c.m. energy range 6.3 GeV $\leqslant\sqrt{s_{NN}}\leqslant$ 200 GeV linearly on the beam rapidity $y_{\rm beam}$ and the saturation-scale exponent λ according to [33]

$$y_{\rm peak} = \frac{1}{1+\lambda}(y_{\rm beam} - \ln A^{1/6}) + \text{const.}, \qquad (7)$$

and, hence, at the current LHC energy of 5.02 TeV PbPb corresponding to $y_{\rm beam} = \mp\ln(\sqrt{s_{NN}}/m_{\rm p}) = \mp 8.586$ and with a gluon saturation-scale exponent $\lambda \sim 0.2$, one expects $y_{\rm peak} \simeq \mp 6$.

Unfortunately the rapidity region of the peaks at LHC energies will therefore not be accessible for identified protons in the coming years due to the lack of a suitable forward spectrometer at LHC. However, the partonic processes that mediate stopping also contribute to hadron production, so one expects fragmentation events in particle production, albeit with peaks occurring at somewhat smaller absolute rapidities than the ones for stopping.

Whereas in net-baryon (proton) distributions charged baryons produced from the gluonic source cancel out because particles and antiparticles are generated in equal amounts, this is obviously not the case in charged-hadron distributions. Here at sufficiently high energy $\sqrt{s_{NN}} \gtrsim 20$ GeV, three sources contribute and the dependence of their particle content on c.m. energy differs: The fragmentation sources contain $N_{\rm ch}^{qg} \propto \ln(s_{NN}/s_0)$ charged hadrons; the midrapidity-centered source that arises essentially from the interaction of low-x gluons contains $N_{\rm ch}^{gg} \propto \ln^3(s_{NN}/s_0)$ charged hadrons and becomes more important than the fragmentation sources at LHC energies [34].

Since the fragmentation distributions must exist in charged-hadron production because they can be measured separately in net-proton data and the gluonic distribution is known to be present in particle production, with particles and antiparticles produced in equal amounts, the total rapidity distribution for

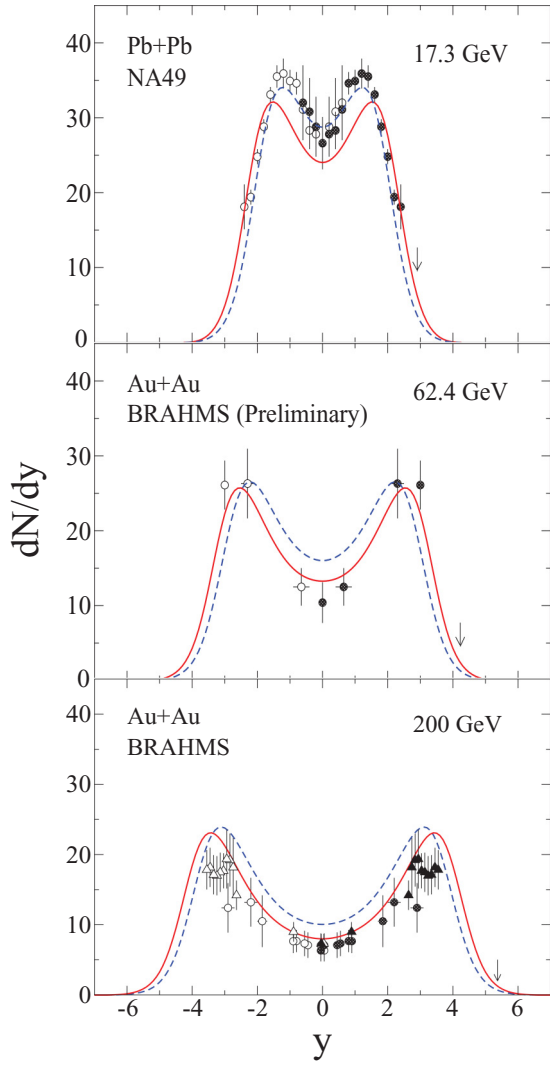

FIG. 3. Evidence for fragmentation sources: Rapidity distributions of net protons in central PbPb collisions at SPS energies of $\sqrt{s_{NN}} = 17.3$ GeV (top frame) compared with NA49 data [31]. Solid curves correspond to a gluon saturation momentum $Q_s = 0.9$ GeV/c at $x = 0.01$, dashed curves to $Q_s = 1.2$ GeV/c. At RHIC energies of 62.4 GeV (middle frame) and 200 GeV (bottom frame) for central AuAu, theoretical results are compared with BRAHMS net proton data [11]. The fragmentation peaks move apart in rapidity space with increasing energy. Arrows indicate the beam rapidities. From Mehtar–Tani and Wolschin [12,32].

produced charged hadrons becomes

$$\frac{dN_{\rm ch}^{\rm tot}(y,t=\tau_{\rm int})}{dy} = N_{\rm ch}^{qg,1} R_1(y,\tau_{\rm int}) + N_{\rm ch}^{gq,2} R_2(y,\tau_{\rm int}) + N_{\rm ch}^{gg} R_{gg}(y,\tau_{\rm int}), \quad (8)$$

with fragmentation distributions $R_{1,2}(y,t)$ and gluonic distributions $R_{gg}(y,t)$ calculated in a time-dependent phenomenological model, such as the relativistic diffusion model (RDM) [35], or in microscopic theories. At the interaction time $t = \tau_{\rm int}$, the strong interaction ceases to act and theoretical distributions may be compared with data in a χ^2 minimization.

In the relativistic diffusion model [35], the initial distribution functions are evolved up to $\tau_{\rm int}/\tau_y$ with the rapidity relaxation time τ_y by using the analytical moments equations. The mean values $\langle y_{1,2}\rangle$ of the fragmentation distributions that are related analytically to $\tau_{\rm int}/\tau_y$ are determined from the data. The absolute value of $\tau_{\rm int}$ does not appear in this calculation because it would require a theory for τ_y, which is not available to date.

The three sources are evolved together, and the equilibration towards the thermal limit for both mean values and widths results from the evolution equation. The widths of the three sources at $\tau_{\rm int}/\tau_y$ are, however, eventually determined empirically in fits to the data because they implicitly include the effect of collective expansion and are therefore considerably larger than the widths that may be calculated from the nonequilibrium evolution equation by using the Einstein relations [36] and are also larger than the thermal limits for the widths. Hence, the evolution equation is governing the statistical equilibration of the mean values of the three sources towards the thermal limit but the widths are empirically found to exceed the thermal values due to collective expansion.

In spite of its reasonable physical basis, the description of the nonequilibrium-statistical equilibration process based on three sources that evolve with time in rapidity space is a macroscopic idealization. This becomes especially evident when two of the three contributions become comparable, as occurs, e.g., in 5 TeV PbPb collisions at rapidity $y \simeq 4$: It seems not obvious why hadrons from valence quark-gluon (fragmentation) events should be out of equilibrium with respect to those from gluon-gluon events at any particular rapidity value. This is, however, different when considering the overall distribution of fragmentation and gluonic events in rapidity space and, in particular, the time evolution of their mean values and widths: The nonequilibrium-statistical view should not be applied to individual events.

Since pseudorapidity distributions $dN/d\eta$ with $\eta = -\ln[\tan(\theta/2)]$ depend only on the scattering angle θ and do not require particle identification; they are easier to obtain at large η values (small scattering angles) compared with rapidity distributions at large values of $y = 0.5$ $\ln[(E + p_\parallel)/(E - p_\parallel)]$. To assess the significance of the fragmentation sources in particle production at LHC energies, it is therefore better to compare theoretical models with pseudorapidity distributions of produced charged hadrons, rather than rapidity distributions of identified particles.

IV. PSEUDORAPIDITY DISTRIBUTIONS

For produced charged hadrons in relativistic heavy-ion collisions, the pseudorapidity distributions $dN_{\rm ch}/d\eta$ thus emerge from a superposition of the fragmentation sources and a midrapidity source that is essentially due to low-x gluons and rises rapidly in particle content according to $N_{gg} \propto \ln^3(s_{NN}/s_0)$ [34]. The Jacobian that accounts for the conversion of rapidity distributions $dN_{\rm ch}/dy$ obtained in any theoretical model to pseudorapidity distributions $dN_{\rm ch}/d\eta$ can

be calculated as

$$\frac{dN}{d\eta} = \frac{dN}{dy}\frac{dy}{d\eta} = J(\eta,m/p_{\rm T})\frac{dN}{dy}, \quad (9)$$

$$J(\eta,m/p_{\rm T}) = \cosh(\eta)[1+(m/p_{\rm T})^2+\sinh^2(\eta)]^{-1/2}, \quad (10)$$

with the hadron mass m and the transverse momentum $p_{\rm T}$. Rather than calculating the Jacobian for charged-hadron distributions with an average mass $\langle m\rangle$ and an average transverse momentum $\langle p_{\rm T}\rangle$, it is more precise to fix the mass m at the pion mass m_π and calculate a corresponding effective mean transverse momentum from $\langle p_{\rm T,eff}\rangle = m_\pi J_{y=0}/(1-J_{y=0}^2)^{1/2}$ [15]. In this expression the Jacobian $J_{y=0}$ at midrapidity is taken from experiment for pions, kaons, and protons.

The effective transverse momenta are smaller than the mean transverse momenta determined from the $p_{\rm T}$ distributions, and the corresponding effect of the Jacobian is therefore larger than that estimated with $\langle p_{\rm T}\rangle$ taken from the transverse momentum distributions for each particle species. At high RHIC and LHC energies, the effect of the Jacobian transformation remains, however, essentially confined to the midrapidity source.

There exist meanwhile several investigations that are considering or incorporating the relevance of the fragmentation sources in rapidity distributions of produced charged hadrons [35,38–41]. In the relativistic diffusion model (RDM) [42,43], the (pseudo-)rapidity distribution of produced particles emerges by construction of the model from an incoherent superposition of the fragmentation components and a third source centered at (or near) midrapidity that is essentially due to low-x gluon-gluon collisions.

All three distribution functions (sources) $R_1(y,t)$, $R_2(y,t)$, and $R_{gg}(y,t)$ evolve in time and are broadened in rapidity space as a consequence of diffusion-like processes governed by a Fokker–Planck equation (FPE). The fragmentation sources tend to shift towards midrapidity due to the drift term. Whereas this drift leads to a sizable overlap of the fragmentation sources at lower [BNL Alternating Gradient Synchrotron (AGS), SPS] energies, their overlap at LHC energies is small due to the large rapidity gap and the very short interaction times; see Fig. 4 for the fragmentation sources in charged-hadron production from 0%–5% central 2.76 TeV PbPb collisions compared with ALICE data [37]. Here dashed curves indicate the time evolution of the fragmentation sources.

The relevance of the fragmentation sources becomes particularly evident when investigating asymmetric systems, such as 200 GeV dAu [43] or 5.02 TeV pPb [47] where the total pseudorapidity distribution becomes asymmetric, is not centered at $\eta = 0$, and depends in a very distinctive manner on centrality. The distributions have steeper slopes in the p-going direction, and the midrapidity source shifts towards the Pb-going direction with increasing centrality. The agreement with the data enhances the credibility of the nonequilibrium three-source approach.

Hence, in the RDM, the equilibration of the fragmentation sources with the gluonic source in the course of time is due to the nonequilibrium-statistical evolution equation [35], with a thermal equilibrium distribution emerging for $t \to \infty$. As is obvious from Fig. 4, the charged-hadron distributions at LHC energies remain far from equilibrium. This is in spite of the

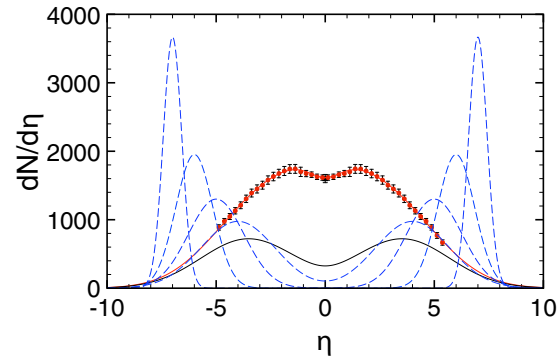

FIG. 4. Fragmentation sources for charged-hadron production in $\sqrt{s_{NN}} = 2.76$ TeV PbPb collisions ($y_{\rm beam} = \mp 7.987$). Solid curves are from a χ^2 minimization of analytical solutions in the relativistic diffusion model (RDM) [35] with respect to the ALICE data [8,37] (upper curve includes the gluonic source, lower curve is for fragmentation sources only). Dashed curves indicate the time evolution of the fragmentation sources in the RDM. The fragmentation sources remain far from equilibrium at LHC energies.

observation that the three subdistributions are close to or have even reached local equilibrium, with an additional broadening due to collective expansion.

In fact, the phenomenological model of Liu *et al.* [40]—after its update from four to three sources according to those discussed here—yields good fits of $dN/d\eta$ data in a large energy range from 19.6 GeV to 2.76 TeV with the assumption of local equilibrium in the three sources. There the midrapidity source is described in the Landau model [48,49]. Since the widths of the three sources have statistical and expansion contributions, it is, however, difficult to determine from the data whether local equilibrium is actually reached in each source.

This result relates to the current intense theoretical investigations of local equilibration within the gluonic source; see, e.g., Refs. [50–52] and references therein. These works concern the microscopic equilibration mechanisms and eventually aim at at fully QCD-based nonperturbative description. A direct connection to the macroscopic investigation of equilibration among the three sources that is presented here is difficult to perform conceptually and mathematically.

The dependence of the pseudorapidity distributions on c.m. energy in central AuAu collisions at 19.6, 130, and 200 GeV RHIC energies as well as in PbPb at 2.76 and 5.02 TeV LHC energies is shown in Fig. 5. In addition to RDM calculations with parameters for the lower energies from Ref. [35] compared with data from Refs. [8,44,45], an extrapolation to 5.02 TeV PbPb with parameters from Table I is compared with a recent midrapidity ALICE data point at 0%–5% centrality [46].

At the lowest RHIC energy of 19.6 GeV that is shown here—which is comparable to the highest SPS energy in the upper frame of Fig. 3—only the fragmentation sources contribute (see dashed curves), but at higher energies the gluonic source rapidly catches up and becomes the largest source of particle production at an energy of ~2 TeV, between energies reached at RHIC and LHC.

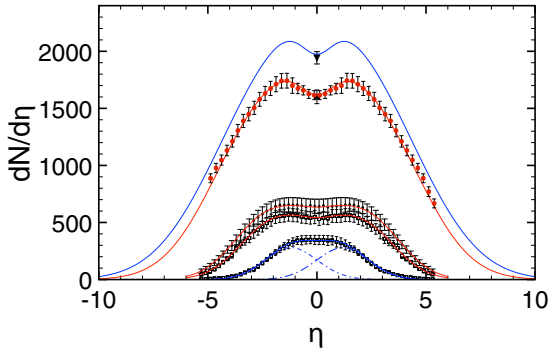

FIG. 5. The RDM pseudorapidity distribution functions for charged hadrons in central AuAu (RHIC) and PbPb (LHC) collisions at c.m. energies of 19.6, 130, 200 GeV, and 2.76 TeV shown here are optimized in χ^2 fits with respect to the PHOBOS [44,45] (bottom) and ALICE [8,37] (top) data, with parameters from Ref. [35]. The upper distribution function at 5.02 TeV is an extrapolation within the relativistic diffusion model. The 5.02 TeV midrapidity data point is from ALICE [46].

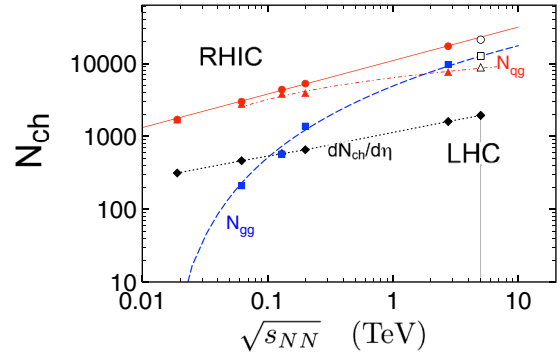

FIG. 6. The total charged-hadron production in central AuAu and PbPb collision in the energy region 19.6 GeV to 5.02 TeV is following a power law (solid upper line), whereas the particle content in the fragmentation sources is $N_{qg} \propto \ln(s_{NN}/s_0)$; dash-dotted curve. The particle content in the midrapidity source obeys $N_{gg} \propto \ln^3(s_{NN}/s_0)$; dashed curve. The energy dependence of the measured midrapidity yields is shown as a dotted line, with PHOBOS data [45] at RHIC energies, and ALICE data [18,46] at 2.76 and 5.02 TeV. The vertical line indicates 5.02 TeV.

The functional dependence of the particle content of the three sources on center-of-mass energy per particle pair $\sqrt{s_{NN}}$ has been investigated in Ref. [34]. For $\sqrt{s_{NN}} \lesssim 20$ GeV the gluonic source is absent (19.6 GeV AuAu PHOBOS result in Fig. 5) and charged-hadron production arises from the fragmentation sources which overlap in rapidity space and hence appear like a single Gaussian ("thermal") source. Experimentally, the total charged-hadron production at these low energies has been found to depend linearly on $\ln(s_{NN}/s_0)$; see, for example, central PbPb NA50 data at 8.7 and 17.3 GeV [53] together with low-energy AuAu PHOBOS results [44].

In the RDM-analysis with three sources [34], it turns out that the dependence of the fragmentation sources $N_{\rm ch}^{qg} \propto \ln(s_{NN}/s_0)$ indeed continues at higher energies up to the present maximum value for PbPb at 5.02 TeV; see Fig. 6. The gluonic source, however, has a much stronger energy dependence $N_{\rm ch}^{gg} \propto \ln^3(s_{NN}/s_0)$ [34]. The rise of the cross section in the central distribution is driven by the growth of the gluon density at small x, and theoretical arguments [54] suggest a $\ln^2 s$ asymptotic behavior that satisfies the Froissart bound [55]. Since the beam rapidity is $\propto \ln(s_{NN})$, the integrated yield from the gluonic source then becomes proportional to $\ln^3 s$. There exist also further experimental confirmations of this result at RHIC energies based on STAR data for dijet production, see Ref. [56] and references therein.

The sum of produced charged hadrons integrated over η is then (accidentally) close to a power law $N_{\rm ch}^{\rm tot} \propto (s_{NN}/s_0)^{0.23}$ with $s_0 = 1$ TeV^2, as shown in Fig. 6 for central AuAu and PbPb collisions (upper line). At RHIC energies Busza noticed that the integrated charged-particle multiplicities scale as $\ln^2(s_{NN}/s_0)$ [57,58], but the energy dependence up to LHC energies is found to be even stronger due to the high gluon density. The midrapidity yields for central AuAu and PbPb collisions are

$$\left.\frac{dN_{\rm ch}^{\rm tot}}{d\eta}\right|_{\eta\simeq 0} = 1.15 \times 10^3 (s_{NN}/s_0)^{0.165}, \qquad (11)$$

with $s_0 = 1$ TeV^2 (dotted line, data points from PHOBOS [45] and ALICE [18,46]).

More detailed aspects of the interplay between fragmentation sources and the gluonic source appear when investigating the centrality dependence of charged-hadron pseudorapidity distributions, as has been done in Refs. [43,47] for the asymmetric systems 200 GeV dAu and 5.02 TeV pPb, and in Ref. [35] for 2.76 TeV PbPb. For the newly investigated symmetric system 5.02 TeV PbPb charged-hadron distributions at centralities 20%–30%, 10%–20%, 5%–10%, and 0%–5% are shown in Fig. 7, with RDM parameters in Table I extrapolated from those at lower energy in Ref. [35].

In a 0%–5% central collision, about 20% of the midrapidity yield still arises from the fragmentation sources; at 20%–30% centrality the fragmentation fraction at midrapidity is about 30%. For 20%–30% centrality the three sources are shown separately in Fig. 7. At all centralities, the system remains far from a thermalization of fragmentation sources and the gluonic source: The three sources are separated in pseudorapidity space at freeze-out. Although each of the sources is close to local

TABLE I. Three-source RDM parameters for charged-hadron production extrapolated to 5.02 TeV PbPb with $y_{\rm beam} = \mp 8.586$ at four centralities; see text. Γ is the full width at half maximum (FWHM) of the sources at the interaction time, $N_{\rm ch}$ the corresponding charged-particle content obtained by using the extrapolation formulas of Ref. [34]. The last column gives the experimental midrapidity values from ALICE [46].

Centrality	$\langle y_{1,2}\rangle$	$\Gamma_{1,2}$	Γ_{gg}	$N_{\rm ch}^{1+2}$	$N_{\rm ch}^{gg}$	$\frac{dN}{d\eta}\vert_{\eta\simeq 0}$
0%–5%	∓ 3.5	5.8	6.7	8644	12682	1943 ± 54
5%–10%	∓ 3.5	6.2	6.8	7623	10041	1586 ± 46
10%–20%	∓ 3.5	6.8	6.9	6023	7278	1180 ± 31
20%–30%	∓ 3.5	7.2	7.0	4271	4873	786 ± 20

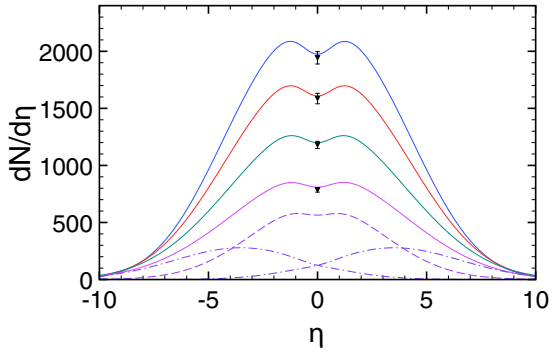

FIG. 7. Pseudorapidity distributions for produced charged hadrons in 5.02 TeV PbPb collisions ($y_{\rm beam} = \mp 8.586$) as functions of centrality, from bottom to top: 20%–30%, 10%–20%, 5%–10%, 0%–5%. Calculated RDM distributions (solid curves) are compared to midrapidity ALICE data from [46]. For 20%–30% centrality, fragmentation and gluonic distribution functions are shown separately.

equilibrium, thermalization would only be reached for very large times that are not accessible at these high energies.

The RDM extrapolations are seen to agree with the midrapidity data points recently measured by ALICE [46]. Small modifications of the parameters may, however, be expected once η-dependent data become available.

For the asymmetric system pPb at the same c.m. energy of 5.02 TeV, pseudorapidity distributions of produced charged hadrons have been analyzed previously in the three-source model at various centralities [47]. The calculated yields are higher in the Pb-going direction ($\eta > 0$ in this plot) than in the p-going direction; see Fig. 8.

The underlying gluonic rapidity distributions are centered at the equilibrium values in the respective centrality bins which are calculated from energy-momentum conservation. The corresponding pseudorapidity distributions that are shown in the figure have a dip at midrapidity due to the Jacobian transformation (9) from rapidity to pseudorapidity space. The slopes of the tails depend on centrality, but they are always steeper on the proton-going side. Particle creation from a gluon-dominated source, in addition to the sources related to the valence part of the nucleons, had also been proposed by Bialas and Czyż [59].

A comparison (χ^2 minimization) with the final ALICE data [9] is shown in Fig. 8, now with the additional constraint [43,60] that the numbers of produced charged hadrons in the fragmentation sources are proportional to the numbers of participants. Again, the distribution functions remain far from thermal equilibrium at all centralities; they do not merge into a single thermal distribution.

The three-source model is related to hydrodynamics and, in particular, to viscous hydrodynamics which also merely assumes local thermal equilibrium, with many three-dimensional (3D) models [23,24] being able to describe the pseudorapidity distributions of charged hadrons. To treat the stopping phase in the initial stage of the collision in viscous hydrodynamics with the ensuing nonequilibrium distribution of baryon-rich matter one needs—similarly to the RDM—a three-source model with two counter-streaming fluids corresponding to the constituent nucleons of the projectile and target nuclei [61,62], and a third

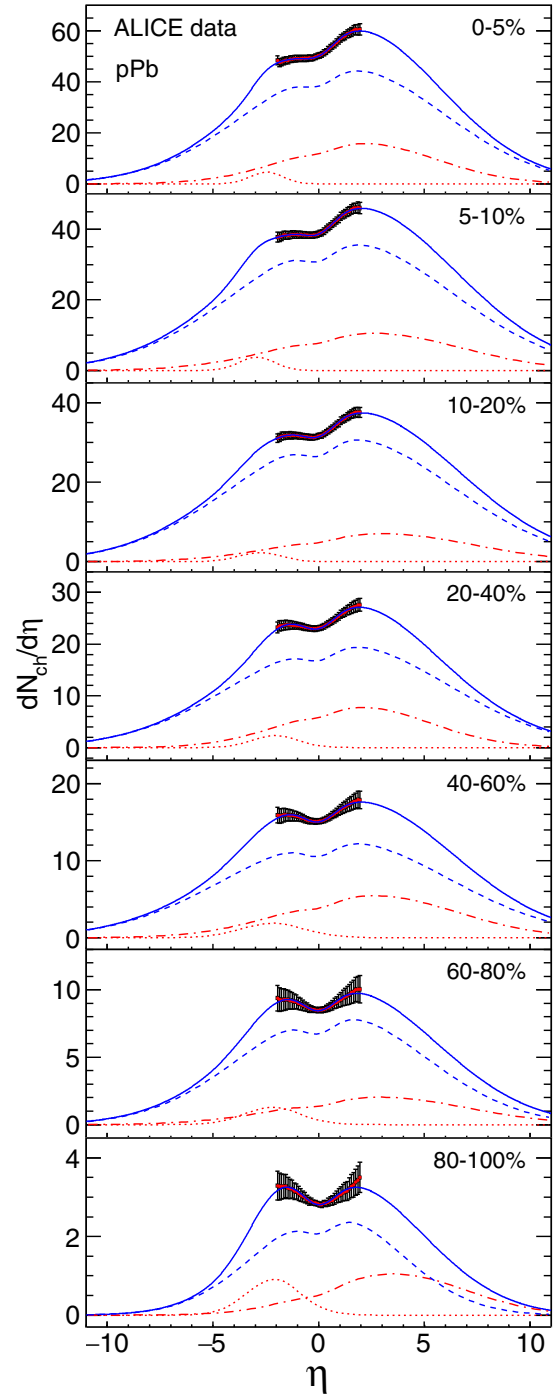

FIG. 8. The centrality-dependent RDM pseudorapidity distribution functions for charged hadrons in pPb collisions at LHC c.m. energy of 5.02 TeV [47] are adjusted in the midrapidity region to the ALICE data [9] through χ^2 minimizations. The underlying distributions in the three–source model are also shown, with the dashed curves arising from gluon-gluon collisions, the dash-dotted curves from valence quark-gluon events in the Pb-going region ($y > 0$ in this plot), and the dotted curves in the p-going direction (fragmentation sources) [60].

source (fireball) in the midrapidity region that is associated with a fluid that is net-baryon free. Corresponding codes have been proposed [63,64] and implemented recently for AuAu

collisions at low energies (BES II program at RHIC) with an emphasis on entropy production and effective viscosity in a three-fluid model using different equations of state for each of the sources with or without deconfinement transition. Such an approach may eventually also be applicable at the much higher LHC energies.

V. CONCLUSION

Deviations from thermal distribution functions for produced particles in relativistic heavy-ion collisions are sensitive indicators for nonequilibrium processes. These are discussed with special emphasis on the respective roles of fragmentation and central fireball sources in the longitudinal degrees of freedom that are quantified in pseudorapidity distributions of produced charged hadrons.

Transverse momentum distributions of produced charged hadrons in heavy-ion collisions at LHC energies are compatible with thermal Maxwell–Juettner distribution functions only at very small $p_T \lesssim 0.5$ GeV/c. In a range 0.5 GeV/$c \lesssim p_T \lesssim$ 7 GeV/c, collective expansion, thermal and nonequilibrium emission of particles contribute, but in a phenomenological model it is difficult to distinguish between the respective contributions.

Above $p_T \sim 7$ GeV/c hard processes are found to take over. These are not amenable to a statistical (equilibrium or nonequilibrium) description but require a pQCD treatment. Due to the rapid fall of the transverse momentum distribution with p_T, the contributions of hard and nonequilibrium processes to the total particle yield remain small when integrated over p_T, although they are relevant for the answer to the question whether the system is in thermal equilibrium.

In the longitudinal degrees of freedom, net-proton rapidity distributions measured at SPS and RHIC energies clearly show the presence of the fragmentation sources in the stopping process. Based on a QCD-inspired model that yields agreement with the data, these distributions result mainly from the interaction of the incoming valence quarks with low-x gluons in the respective other nucleus.

The fragmentation sources are present also in the production of charged hadrons, where they compete with the low-x gluonic source that is centered at midrapidity and rises rapidly in charged-particle content with the cube of the logarithmic c.m. energy. Although all three sources are close to local equilibrium and broadened due to collective expansion, thermalization among them is not achieved during the short interaction time of ∼5–8 fm/c in heavy-ion collisions at LHC energies.

A three-source nonequilibrium-statistical relativistic diffusion model that accounts for the time evolution of the fragmentation sources and the gluonic midrapidity source shows that the system remains far from thermal equilibrium among the sources, which would be reached only for large times $t \to \infty$. The model is used to predict pseudorapidity distributions and their centrality dependence for symmetric systems such as 5.02 TeV PbPb; it is also applicable for asymmetric systems such as pPb.

In both cases and at all centralities the distribution functions remain far from thermal equilibrium distributions due to the large rapidity gap and the short interaction times of about 10^{-23} s at energies reached at the Relativistic Heavy Ion Collider (RHIC) and the Large Hadron Collider (LHC).

ACKNOWLEDGMENTS

I am grateful to Jean–Paul Blaizot, Kenji Fukushima, Larry McLerran, and Raju Venugopalan for conversations about local equilibration during their stays at the Heidelberg Institute for Theoretical Physics, and to Frederike Vogel for her participation in the 5.02 TeV calculations. This work is supported by DFG through the Transregional Research Center TRR33 at the Universities of Bonn, LMU Munich, and Heidelberg. I thank my TR colleagues for their cooperation.

[1] R. Hagedorn, Nuovo Cim. Suppl. **3**, 147 (1965).
[2] P. Braun-Munzinger, J. Stachel, J. Wessels, and N. Xu, Phys. Lett. B **344**, 43 (1995).
[3] J. Manninen and F. Becattini, Phys. Rev. C **78**, 054901 (2008).
[4] P. Braun-Munzinger, V. Koch, T. Schaefer, and J. Stachel, Phys. Rep. **621**, 76 (2016).
[5] J. C. Mather *et al.* (COBE Collaboration), Astrophys. J. **354**, L37 (1990).
[6] G. Hinshaw *et al.* (WMAP Collaboration), Astrophys. J., Suppl. Ser. **180**, 225 (2009).
[7] R. Adam *et al.* (Planck Collaboration), Astron. Astrophys. (to be published).
[8] E. Abbas *et al.* (ALICE Collaboration), Phys. Lett. B **726**, 610 (2013).
[9] J. Adam *et al.* (ALICE Collaboration), Phys. Rev. C **91**, 064905 (2015).
[10] B. Cole *et al.* (ATLAS Collaboration), ATLAS-CONF-2013-096 (2013).
[11] I. G. Bearden *et al.* (BRAHMS Collaboration), Phys. Rev. Lett. **93**, 102301 (2004).
[12] Y. Mehtar-Tani and G. Wolschin, Phys. Rev. Lett. **102**, 182301 (2009).
[13] F. O. Durães, A. V. Giannini, V. P. Gonçalves, and F. S. Navarra, Phys. Rev. C **89**, 035205 (2014).
[14] F. Jüttner, Ann. Phys. (Berlin, Ger.) **339**, 856 (1911).
[15] D. M. Röhrscheid and G. Wolschin, Phys. Rev. C **86**, 024902 (2012).
[16] T. Kind and G. Wolschin (private communication).
[17] B. Abelev *et al.* (ALICE Collaboration), Phys. Lett. B **720**, 52 (2013).
[18] K. Aamodt *et al.* (ALICE Collaboration), Phys. Rev. Lett. **106**, 032301 (2011).
[19] I. G. Bearden *et al.* (NA44 Collaboration), Phys. Rev. Lett. **78**, 2080 (1997).
[20] P. J. Siemens and J. O. Rasmussen, Phys. Rev. Lett. **42**, 880 (1979).

[21] E. Schnedermann, J. Sollfrank, and U. Heinz, Phys. Rev. C **48**, 2462 (1993).
[22] U. Heinz and R. Snellings, Annu. Rev. Nucl. Part. Sci. **63**, 123 (2013).
[23] C. Gale, S. Jeon, and B. Schenke, Int. J. Mod. Phys. A **28**, 1340011 (2013).
[24] R. D. de Souza, T. Koide, and T. Kodama, Prog. Part. Nucl. Phys. **86**, 35 (2016).
[25] R. Hagedorn, Riv. Nuovo Cimento **6**, 1 (1983).
[26] C. Y. Wong and G. Wilk, Phys. Rev. D **87**, 114007 (2013).
[27] W. M. Alberico, A. Lavagno, and P. Quarati, Eur. Phys. J. C **12**, 499 (2000).
[28] C. Tsallis, J. Stat. Phys. **52**, 479 (1988).
[29] R. Balian and M. Nauenberg, Europhys. News **37**, 9 (2006).
[30] J. D. Bjorken, Phys. Rev. D **27**, 140 (1983).
[31] H. Appelshäuser *et al.* (NA49 Collaboration), Phys. Rev. Lett. **82**, 2471 (1999).
[32] Y. Mehtar-Tani and G. Wolschin (private communication).
[33] Y. Mehtar-Tani and G. Wolschin, Europhys. Lett. **94**, 62003 (2011).
[34] G. Wolschin, Phys. Rev. C **91**, 014905 (2015).
[35] G. Wolschin, J. Phys. G **40**, 45104 (2013).
[36] G. Wolschin, Europhys. Lett. **47**, 30 (1999).
[37] M. Guilbaud *et al.* (ALICE Collaboration), Nucl. Phys. A **904**, 381c (2013).
[38] R. Sahoo and A. N. Mishra, Int. J. Mod. Phys. E **23**, 1450024 (2014).
[39] R. Sahoo, A. N. Mishra, N. K. Behera, and B. K. Nandi, Adv. High Energy Phys. **2015**, 612390 (2015).
[40] L.-N. Gao and F.-H. Liu, Adv. High Energy Phys. **2015**, 184713 (2015).
[41] E. K. G. Sarkisyan, A. N. Mishra, R. Sahoo, and A. S. Sakharov, Phys. Rev. D **93**, 054046 (2016).
[42] G. Wolschin, Eur. Phys. J. A **5**, 85 (1999).
[43] G. Wolschin, M. Biyajima, T. Mizoguchi, and N. Suzuki, Phys. Lett. B **633**, 38 (2006).
[44] B. B. Back *et al.* (PHOBOS Collaboration), Phys. Rev. Lett. **91**, 052303 (2003).
[45] B. Alver *et al.* (PHOBOS Collaboration), Phys. Rev. C **83**, 024913 (2011).
[46] J. Adam *et al.* (ALICE Collaboration), Phys. Rev. Lett. **116**, 222302 (2016).
[47] P. Schulz and G. Wolschin, Eur. Phys. J. A **51**, 18 (2015).
[48] L. D. Landau, Izv. Akad. Nauk. Ser. Fiz. **17**, 51 (1953).
[49] S. Z. Belen'kji and L. D. Landau, Usp. Fiz. Nauk **56**, 309 (1955).
[50] L. McLerran, Nucl. Phys. A **926**, 3 (2014).
[51] R. Venugopalan, Nucl. Phys. A **928**, 209 (2014).
[52] K. Fukushima, Rep. Prog. Phys. (to be published).
[53] F. Prino *et al.* (NA50 Collaboration), J. Phys.: Conf. Ser. **5**, 86 (2005).
[54] M.-F. Cheung and C. B. Chiu, arXiv:1111.6945.
[55] M. Froissart, Phys. Rev. **123**, 1053 (1961).
[56] T. Trainor and D. J. Prindle, Phys. Rev. D **93**, 014031 (2016).
[57] W. Busza, Acta Phys. Polon. B **35**, 2873 (2004).
[58] W. Busza, J. Phys. G **35**, 044040 (2008).
[59] A. Bialas and W. Czyż, Acta Phys. Polon. B **36**, 905 (2005).
[60] P. Schulz and G. Wolschin (private communication).
[61] A. A. Amsden, A. S. Goldhaber, F. H. Harlow, and J. R. Nix, Phys. Rev. C **17**, 2080 (1978).
[62] R. B. Clare and D. Strottman, Phys. Rep. **141**, 177 (1986).
[63] Y. B. Ivanov, V. N. Russkikh, and V. D. Toneev, Phys. Rev. C **73**, 044904 (2006).
[64] Y. B. Ivanov and A. A. Soldatov, arXiv:1605.0247.